



UNIVERSITY OF LEEDS

This is a repository copy of *Ordered structures with Schottky heterojunction functional unit regulate immune response and osteogenesis*.

White Rose Research Online URL for this paper:

<https://eprints.whiterose.ac.uk/225058/>

Version: Accepted Version

Article:

Yu, P., Ran, M., Ran, H. et al. (7 more authors) (2025) Ordered structures with Schottky heterojunction functional unit regulate immune response and osteogenesis. *Journal of Material Science and Technology*, 213. pp. 276-287. ISSN 1005-0302

<https://doi.org/10.1016/j.jmst.2024.05.072>

© 2025 Published by Elsevier Ltd on behalf of The editorial office of *Journal of Materials Science & Technology*. This is an author produced version of an article published in *Journal of Materials Science & Technology* Uploaded in accordance with the publisher's self-archiving policy. This manuscript version is made available under the CC-BY-NC-ND 4.0 license <http://creativecommons.org/licenses/by-nc-nd/4.0/>.

Reuse

This article is distributed under the terms of the Creative Commons Attribution-NonCommercial-NoDerivs (CC BY-NC-ND) licence. This licence only allows you to download this work and share it with others as long as you credit the authors, but you can't change the article in any way or use it commercially. More information and the full terms of the licence here: <https://creativecommons.org/licenses/>

Takedown

If you consider content in White Rose Research Online to be in breach of UK law, please notify us by emailing eprints@whiterose.ac.uk including the URL of the record and the reason for the withdrawal request.



eprints@whiterose.ac.uk
<https://eprints.whiterose.ac.uk/>

Ordered structures with Schottky heterojunction functional unit regulate immune response and osteogenesis

Peng Yu^{a,1*}, Maofei Ran^{a,1}, Heying Ran^{a,1}, Xuebin Yang^c, Youzhun Fan^a, Zhengao Wang^a, Zhengnan Zhou^a, Jinxia Zhai^a, Zefeng Lin^{b,*}, Chengyun Ning^a

^a School of Material Science and Engineering, National Engineering Research Center for Tissue Restoration and Reconstruction, GuangDong Engineering Technology Research Center of Metallic Materials Surface Functionalization, South China University of Technology, Guangzhou 510641, China

^b Guangdong Key Lab of Orthopedic Technology and Implant, General Hospital of Southern Theater Command of PLA, Guangzhou, 510010, China

^c Biomaterials and Tissue Engineering Group, School of Dentistry, University of Leeds, Leeds, LS97TF, UK

* Corresponding authors. School of Material Science and Engineering, South China University of Technology, Guangzhou, 510640, China

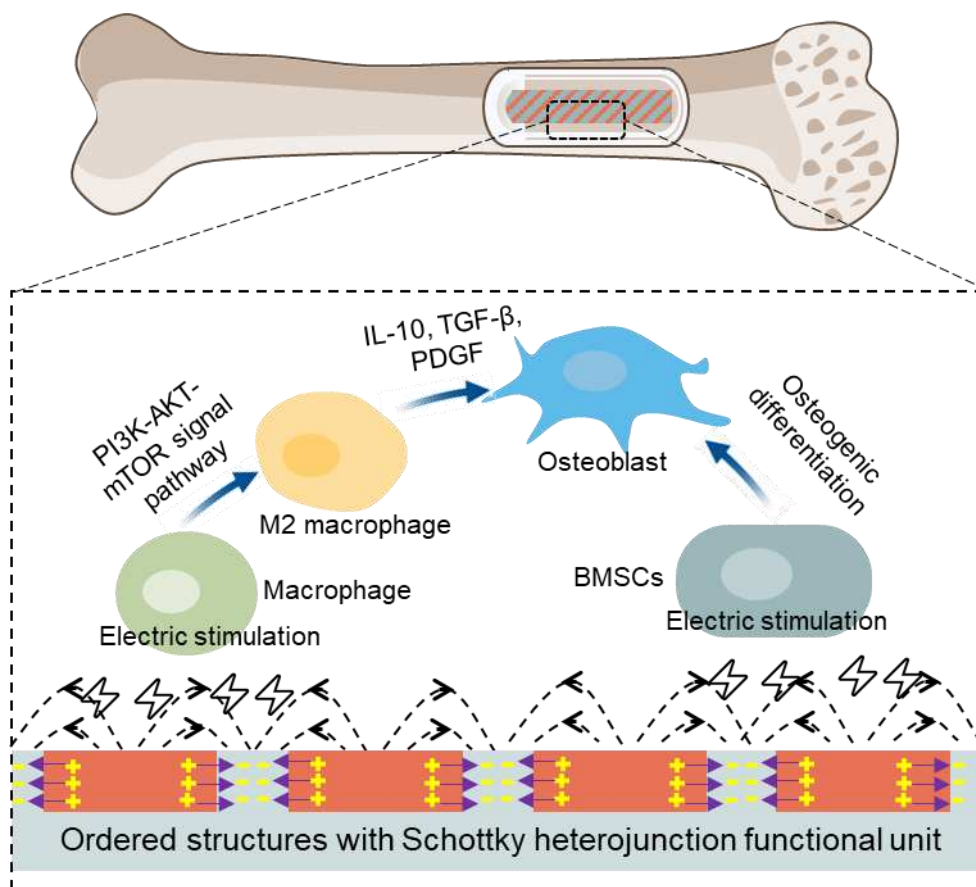
E-mail: imyup@scut.edu.cn (P. Yu)

* General Hospital of Southern Theater Command of PLA, Guangzhou, 510010, China

E-mail: lzefeng_scut@126.com (Z. Lin)

¹ These authors contributed equally to this work.

Graphical abstract



The ordered structures with Schottky heterojunction functional unit are developed to provide a unique electric microenvironment on implant to activate PI3K-AKT-mTOR signaling pathway of macrophages and promote bone regeneration.

Abstract

Mimicking the electric microenvironment of natural tissue is a promising strategy for developing biomedical implant. However, current researches have not taken biomimetic electrical functional units into consideration when designing biomedical implant. In this research, ordered structures with Schottky heterojunction functional unit (OSSH) were constructed on titanium implant surface for bone regeneration regulation. The Schottky heterojunction functional unit is composed of periodically distributed titanium microdomain and titanium oxide microdomain with different carrier densities and surface potentials. The OSSH regulates the M2-type polarization of macrophages to a regenerative immune response by activating PI3K-AKT-mTOR signal pathway, and further promotes osteogenic differentiation of rat bone marrow mesenchymal stem cells. This work provides fundamental insights into the biological effects driven by the Schottky heterojunction functional units that can electrically modulate osteogenesis.

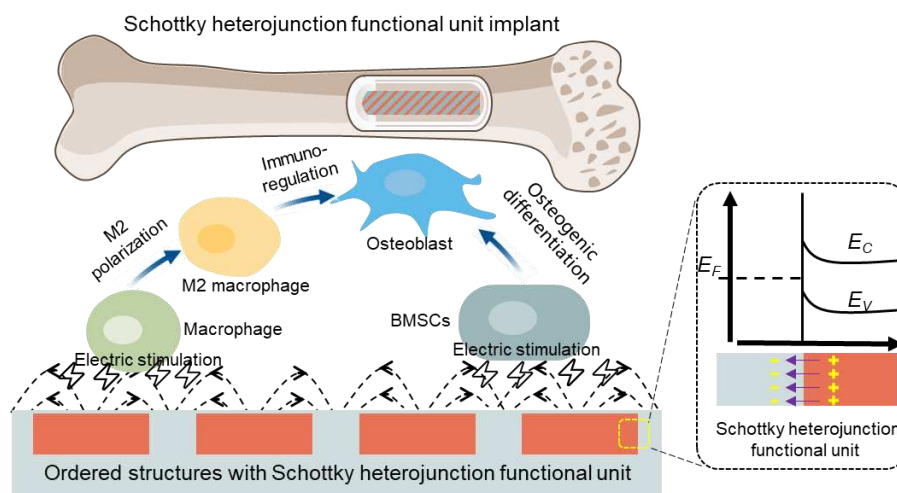
Keywords: ordered structures with functional unit; macrophage; implant; osteogenesis; electric microenvironment

1. Introduction

Electrical communication and signal transduction within cells and tissues control gene expression and cell behavior [1, 2]. Traditionally, electrical stimulation is applied to the tissue defect by external electrical stimulation to promote tissue healing [3, 4]. In recent years, thanks to the rapid development of electroactive biomaterials, the modulation of the intrinsic electrical properties of biomaterials to regulate cell behavior and tissue regeneration is drawing increasing attention [5-7]. The intrinsic electric stimulation from biomaterials to the cells and tissues can mimic the electric microenvironment of the natural tissue to promote tissue regeneration [8]. Although the research on the electrical properties of materials and cell interactions is gradually deepening, what kind of materials electrical properties is conducive to regulate tissue regeneration is still perplexing scientists. Actually, human tissues are composed by an optimized order structures with electric functional units [9, 10]. The basic bone tissue unit, Haversian system, is composed by order structures with piezoelectric functional units, providing the electric microenvironment of bone [11, 12]. However, most current electroactive bone implant materials are developed based on the manipulation of atoms or molecules without considering these ordered structures with electrical functional units.

The material design concept of material elementary order structure with functional units provides a new perspective for this research [13]. This project proposed to develop electrical functional unit with order structure on titanium-based bone implant material, one of the most widely used biomaterials in clinical applications [14]. Titanium is a metal, but the surface of titanium can be oxidized to form a titanium oxide semiconductor structure. Schottky heterojunction is a semiconductive functional unit which is constructed via direct contact between metal and semiconductor. Because the work function between the metal and the semiconductor are different in Schottky heterojunction, potential difference

will generate when the metal is in contact with the semiconductor. Schottky heterojunction functional units can be constructed by selectively oxidizing microdomains on titanium surfaces. In this research, we propose to construct ordered structures with Schottky heterojunction functional unit (OSSH) on titanium implant (Scheme 1). In order to construct OSSH on the titanium surface, we use the selective laser-induced phase change technology to selectively oxidize the microdomains of the titanium surface, thus the titanium oxide semiconductive microdomains and the original pure titanium microdomains periodically distributed to form Schottky heterojunction functional units. The periodic order structure is arranged to form a titanium-based implant material with electrical functional unit, in order to achieve the performance of promoting bone tissue regeneration beyond traditional materials. We found that OSSH materials can promote the anti-inflammatory polarization of immune cells, which is related to order structure with functional unit.



Scheme 1. Ordered structures with Schottky heterojunction functional unit (OSSH) on titanium bone implant materials regulate the M2 polarization of macrophages and osteogenic differentiation of stem cells. OSSH with periodic distribution of titanium oxide functional microdomains (orange color) and titanium metal microdomains (gray color) is constructed on titanium implant. The diagram in the dashed rectangle inset shows the Schottky heterojunction functional unit (E_F : Fermi level, E_C :

Conduction band, E_V : Valence band). In the Schottky heterojunction functional unit, the titanium and titanium oxide microdomains in contact share different work function, thus different surface potential exhibits on titanium and titanium microdomains. The electron density on the metal surface increases, while the positive charge density on the semiconductor surface increases. The OSSH can apply electrical stimulation to cells to regulate the M2-type polarization of macrophages, thereby promoting osteoimmunoregulation as well as the osteogenic differentiation of stem cells.

2. Materials and methods

2.1 Construction of OSSH

Medical titanium sheet (ASTM standard, Qichen, Baoji, China) were ultrasonically cleaned with acetone, ethanol, and deionized water for 20 mins, and dried in a vacuum drying oven before use. Selective laser oxidation treatment was performed using a laser manufacturing machine (HM20, Han's Laser, China) to construct Schottky heterojunction functional unit on titanium implant. Fix the medical titanium sheet on the desktop of the laser marking machine. Set the scanning distance and path via CAD software to control the ordered structure of functional unit, and perform oxidation treatment under the conditions of 3 W power and 100 mm/s scanning speed. For cylindrical titanium implant samples, an attached rotary stepper motor was use to hold the samples to construct heterojunction functional unit. Set the stepper motor speed to match laser scanning frequency.

2.2 Characterization of OSSH

The samples were pasted on the sample stage, and after spraying gold for 60 s, the morphology of the micro-area semiconductor-metal heterojunction was observed using a field emission scanning electron microscope (Merlin, Zeiss, Germany). The working voltage is 10 kV, and the working distance is 5-8 mm. At the same time, the energy spectrum analyzer (EDS) attached to the scanning electron

microscope was used to analyze the changes in element content before and after laser irradiation. An X-ray diffractometer (Empyrean) from PANalytical Company of Holland was used to analyze the phases after laser irradiation. The scanning range 2θ was $10\sim 80^\circ$, and the scanning step length was 0.02° .

2.3 Electrical properties of OSSH

An electrochemical workstation (ZAHNER, ZENNIUM, German) was used to detect the Mott-Schottky curve of the samples, and the carrier density of the sample was calculated using equation (1).

$$C^{-2} = \frac{2(E-E_{fb}-kT/e)}{N_D \epsilon \epsilon_0 e A^2} \quad (1)$$

Where N_D is the electron density, C is the space charge capacitance, E_{fb} is flat band potential, and A is the active surface area. The electron density of the electrode can be calculated from the intercept and the slope, respectively. ϵ is the dielectric constant of titanium oxide, ϵ_0 is the vacuum permittivity, k is the Boltzmann constant, T is the absolute temperature and e is the elementary charge.

A three-electrode system was used in a 0.5 M Na_2SO_4 solution (the sample was the working electrode, and $\text{Ag}|\text{AgCl}$ was the reference electrode, and the platinum electrode is the counter electrode). The sweep range is $-2\text{ V}\sim 2\text{ V}$, and the sweep step size is 0.2 V. The surface potential of the boundary between the laser oxidized microdomain and the unoxidized microdomain was measured by using the SKPM mode of the atomic force microscope (MFP-3D-SA, Asylum Research, US). After the test, use the Igor Pro software to analyze the potential difference between the laser-irradiated area and the non-irradiated area.

2.4 Cell culture

RAW264.7 macrophages and BMSCs were cultured with Dulbecco's modified Eagle's medium containing 10% fetal bovine serum (FBS) and 1% penicillin-streptomycin. When reaching 80%

confluence, trypsinize the cell sheet to obtain a cell suspension. The OSSHs and the control group samples were sterilized by immersing them in 75% medical alcohol under ultraviolet light for 30 mins. A certain concentration of cell suspension was inoculated on the surface of the material and cultured in a cell incubator with a 5% CO₂ atmosphere and a constant temperature of 37°C.

2.5 Cell adhesion and proliferation

RAW264.7 macrophages were seeded on the surface of a 48-well plate at a density of 10,000 cells/well. After culturing for 3 days, the cytoskeleton was stained with Actin-Tracker Green-488 fluorescent probe. And use DAPI staining solution to stain the cell nucleus, and then observe the cytoskeleton under a laser confocal microscope. The CCK-8 kit was used to detect the cell proliferation ability of BMSCs and macrophages. Prepare the working solution according to the ratio of CCK-8 stock solution. After the cells and materials are co-cultured for a certain period of time, aspirate the medium, add 200 µL of working solution to each well, and place it in 5% CO₂. Incubate in a constant temperature incubator at 37 °C for 1 h in the dark. After incubation, use a microplate reader to detect the absorbance at 450 nm.

2.6 Alkaline phosphatase activity detection

ALP activity was detected by ALP kit. Configure the working fluid and operate in accordance with the requirements of the ALP test kit (Beyotime Biotechnology). Incubate the working solution in a 37 °C oven for 30 min. After the incubation, add 100 µL of reaction stop solution to each well to stop the reaction, and detect under the conditions of 405 nm wavelength. Use the BCA protein detection kit to detect the total protein content of the cell lysate, use the microplate reader to measure the absorbance at 562 nm, and calculate the total protein concentration of the sample according to the standard curve; The ALP activity was calculated according to the ALP concentration and total protein concentration.

ALP staining assay was detected by BCIP/NBT Alkaline Phosphatase Color Development Kit (Beyotime Biotechnology). Take out the cells cultured to the time point, add 200 μ L of 4% paraformaldehyde to each well and fix for 30 min at room temperature. Configure BCIP according to the requirements of the alkaline phosphatase staining kit/NBT staining working solution, just add working solution to the cell sample, incubate at 37 °C for 30 min, wash with distilled water to stop the color reaction, take pictures under a stereo microscope (SteREO Discovery.V20, Zeiss, Germany).

2.7 RT-qPCR to detect the expression of inflammation and osteogenic genes

After RAW264.7 macrophages or bone marrow mesenchymal stem cells are cultured on the surface of the material for a certain period of time, the cells are lysed with RL Buffer lysis solution, transferred to a centrifuge tube, and filtered. The column kit collects and purifies RNA. Reverse transcription of RNA into cDNA was performed using a reverse transcription kit (Takara Bio Inc., Japan). Quantitative real-time polymerase chain reaction analysis was performed using the SYBR Green PCR reagent on an ABI Prism 7300 system (Applied Biosystems, Foster City, CA). The primer sequences of macrophage and osteogenic genes are shown in Table S1-3. glyceral triphosphate dehydrogenase (GAPDH) Glyceraldehyde-3-phosphate dehydrogenase served as the housekeeping gene. The expression of PI3K/AKT/mTOR related genes on the surface of different materials was also detected by RT-qPCR.

2.8 Immunofluorescence staining of inflammation-related proteins and osteogenic-related proteins

Inoculate RAW264.7 macrophages and BMSCs on the surface of OSSH material. Add 4% paraformaldehyde for fixation, 0.1% TritonX-100/PBS for permeabilization and 3% BSA/PBS solution for blocking at 4 °C, sequentially. Then the samples were incubated with primary antibodies

iNOS (1:200, Abcam) and Arg-1 (1:200, Abcam) overnight at 4 °C in the dark. Secondary antibody goat Anti-Rabbit Alexa Fluor 594 and Actin-Tracker Green were used for linking the primary antibody and staining actin fiber, respectively. DAPI staining solution was used to stain nucleus. The fluorescence images were acquired by Confocal laser scanning microscope (CLSM). YAP nuclear localization protein immunofluorescence staining was used to detect its expression on the surface of different materials.

2.9 Flow cytometry to detect macrophage phenotype

Flow cytometry was used to detect the expression of CCR7 and CD206. RAW264.7 macrophage cells were seeded on the surface of a 48-well plate at a density of 10,000 cells/well. After culturing for 3 days, the cell suspension was centrifuged and blocked with 1% BSA/PBS at 4°C for 30 min. Then add 200 µL (100 µL CCR7+100 µL CD206) antibody working solution, and incubate for 1 h at 4 °C in the dark after the addition. After incubation, centrifuge and resuspend the cells, and transfer to a flow cytometer (Guava easycyte, Millipore, USA) for testing ; Use FlowJo software to analyze the positive part of RAW264.7 macrophage M1 and M2 populations on the cell surface of each group.

2.10 Intracellular calcium ions detection

The fluorescent probe of the calcium ion concentration in Fluo-4 AM cells was used to stain and analyze the calcium ions in macrophages and BMSCs. After incubation, the as-prepared Fluo-4 AM (Beyotime Biotechnology) working solution was added to the surface of the cell sample. Incubate at 37 °C in the dark for 30 min to load the fluorescent probe. Use a laser confocal microscope to detect at a wavelength of 488 nm.

2.11 Macrophage immunopolarization signaling pathway

Osteogenic differentiation of BMSCs co-cultured in macrophage-conditioned medium: Macrophages

were seeded on the surface of the samples. After 3 days of culture, the macrophage medium was collected, centrifuged to remove the cell debris, and the supernatant were obtained. The supernatant and DMEM complete medium were made into macrophage conditioned medium at a ratio of 1:1. Use this macrophage conditioned medium to culture BMSCs for 7 days for immunofluorescence staining and alkaline phosphatase activity analysis.

2.12 *In vivo* implantation experiment

The animals used in this experiment are SD rats aged 6-8 weeks. The experiment was approved by the Experimental Animal Ethics Committee of the PLA General Hospital of Southern Theater Command (the assigned approval number: 20201124-1). The material implantation and removal experiments were carried out in the Animal Experiment Center of the General Hospital of Southern Theater Command. First, the rats were anesthetized by intraperitoneal injection of 3% pentobarbital sodium. After the anesthesia was completed, the hair on the femur of the hind leg was removed with a razor. After the iodophor disinfection, the muscle tissue was cut parallel to the femur, and the bone surface was exposed. And then a low-speed orthopedic drill was used to acquire a bone defect with a diameter of 2 mm along the direction parallel to the femur to the bone marrow cavity. The samples were implanted into the femoral defect and suture the wound after iodophor disinfection. After suturing, 100,000 units of penicillin were injected into the leg muscle tissue, and the injection continued for 3 days after the operation. Finally, after 6 weeks of feeding, all rats were killed by CO₂ asphyxiation, the muscle tissue and soft tissue around the femur were stripped to obtain the entire femur containing the implant, and the femur was soaked in 4% paraformaldehyde for fixation.

2.13 Micro-CT three-dimensional image reconstruction

Take out the entire femur specimen containing the implant, put it into the Micro-CT (XTV160H)

scanning stage, set the working parameters: voltage/current: 101 kV/53 μ A; exposure time: 250 ms.

After obtaining the data, use VGStudio MAX software to build a three-dimensional model, analyze bone volume/total volume (BV/TV), average trabecular thickness (Tb.Th), average trabecular number (Trabecular number, Tb.N) and average trabecular separation (Tb.Sp).

2.14 Tissue section staining

After fixing, dehydrating, transparent, embedding, and sectioning the femoral specimen containing the implant, a 5-10 μ m section is obtained, which is attached to a clean glass slide, and then stained with hematoxylin and eosin Stain in H&E and Masson dye solution for 5 min. After staining, take out the section, dry the surface dye solution, place it in 95% alcohol, remove non-specific staining, and use a multifunctional vertical microscope (Leica DM4000 M) to observe the section after drying.

Statistical analysis: Data are presented as mean \pm standard deviation (SD). Statistically significant differences were measured using one-way analysis of variance (ANOVA) and Tukey's multiple comparison test. Statistical analysis was performed using SPSS (International Business Machines Corporation, US) software.

3. Results and discussion

3.1 Characterization of OSSH

In order to build ordered structures with Schottky heterojunction functional units on implant materials, titanium oxide semiconductive microdomains were constructed on titanium implant using laser microdomain oxidation, a fast and efficient regional surface treatment technology with laser producing high temperatures in the focus area. Thereby oxidized microdomain can be easily and efficiently constructed on titanium implant to fabricate Schottky heterojunction functional unit on implant material. Scanning electron microscopy (SEM) images showed that a heterojunction with ordered

distribution features was constructed on titanium (Fig. 1a), and the period of the heterojunction could be fine-tuned by adjusting the site-selective laser oxidation strategy via computer aided program (Fig. S1). Quantitative analysis indicates that the width of the laser-oxidized microdomain is $13.31 \pm 0.26 \mu\text{m}$, while the other parts remain untreated. The Energy Dispersive Spectrometer (EDS) mapping results showed that oxygen and titanium elements were ordered distributed on the surface of the implanted material after treatment, with a higher oxygen content on the laser oxidized microdomains (Fig. 1b, c). XRD analysis results showed that the laser oxidized area was mainly composed of TiO phases (Fig. 1d). The Mott Schottky curve proved that laser oxidized zone was an n-type semiconductor with a carrier density of $20.805 \times 10^{20} \text{ cm}^{-3}$ (Fig. 1e). As demonstrated by Scanning Kelvin Probe Force Microscopy (SKPFM) that this Schottky heterojunction functional unit material formed a microdomain potential difference, and the potential of the titanium oxide microdomain was about $\sim 50 \text{ mV}$ higher than that of the pure titanium microdomain (Fig. 1f), which further confirmed OSSH construction on titanium implant.

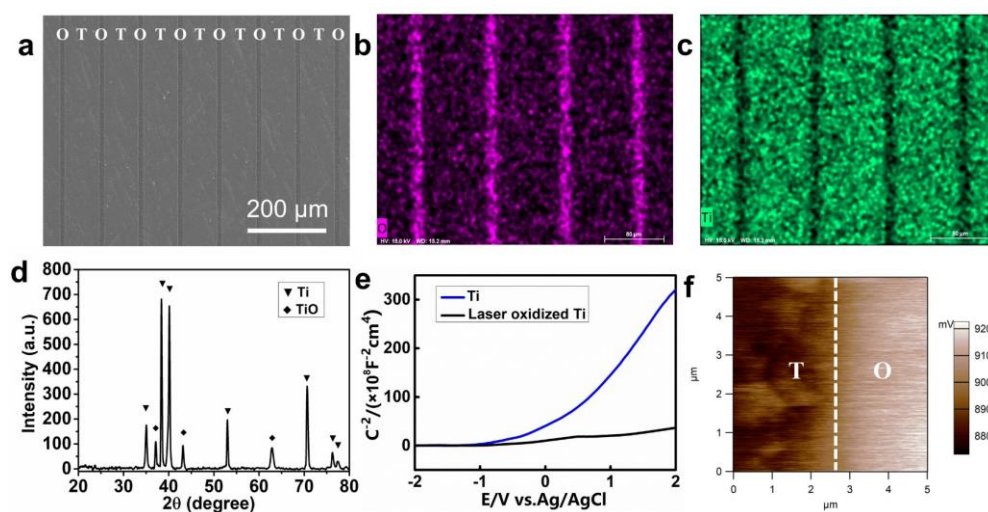


Fig. 1. Characterization of OSSH material. (a) SEM image of OSSH, T: Ti microdomain, O: titanium oxide microdomain. (b) and (c) EDS oxygen and titanium element mapping of OSSH, respectively. (d) XRD pattern of laser oxidized Ti. (e) The Mott-Schottky curve of Ti and laser oxidized Ti. (f) SKPFM

image of the surface potential distribution between OSSH microdomain boundaries. Left: Titanium microdomain. Right: Titanium oxide microdomain. The above results indicate that ordered structures with Schottky heterojunction functional unit is constructed on titanium implant.

3.2 OSSH regulates osteogenic differentiation

To assess the biological response of OSSH, the rat bone marrow mesenchymal stem cells (BMSCs) were cultured on OSSHs and the controls. The research groups were set as OSSH with microdomain interval of 100 μm (OSSH-100), OSSH with microdomain interval of 50 μm (OSSH-50), OSSH with microdomain interval of 30 μm (OSSH-30), titanium and oxidized titanium whose surface is completely oxidized by laser irradiation. The cytoskeleton of BMSCs cultured on the surface of the OSSH and control groups was evaluated via fluorescent staining. The CLSM image of cytoskeleton microfilament (green) showed that the cells on OSSHs surface spread well and were larger than that of the cells cultured on the titanium and oxidized titanium group (Fig. S2). Furthermore, the cell spread area of cells on OSSH groups increased with decreasing microdomain interval, suggesting that the size range of the heterojunction functional unit structure has a regulatory effect on cell adhesion. The cell counting kit-8 (CCK-8) assay was used to determine the regulatory effect of OSSH on BMSCs proliferation. The evaluation results showed that the proliferative properties of the cells cultured on OSSH surface were enhanced compared to the controls (Fig. S2f). And on the first day of cell culture, there was no significant difference in the cell proliferation rate between the experimental group and the titanium group. On day 4, the cell viability of OSSH-100 was slightly higher than that of Titanium group, while the cell activity of OSSH-50 and OSSH-30 group was higher than that of OSSH-100 group. On the 7th day of culture, the cell viability of all OSSH groups and oxidized titanium groups was significantly higher than that of titanium group. CCK-8 results indicated that the OSSH titanium

implant material is biocompatible, and it promotes cell proliferation compared to control groups.

To study the regulatory of Schottky heterojunction functional unit on the osteogenic process, the expression level of alkaline phosphatase (ALP), which is closely related to the osteogenic differentiation of stem cells, was used to evaluate the BMSCs osteogenic differentiation performance on OSSHs and controls. The results showed that the ALP expression level of BMSCs cells on the surface of the Schottky heterojunction unit titanium materials was higher than that of the control group after co-cultivation for 7 days, and the cell enzyme expression level on the OSSH-30 surface was the highest, indicating that this group of materials had the strongest ability to promote the secretion of ALP by cells. Quantitative analysis results further confirmed the above results (Fig. S3). The above results preliminarily demonstrate that the Schottky heterojunction functional unit can promote the osteogenic differentiation of cells. Further immunofluorescence staining was used to evaluate Runt-related transcription factor 2 (Runx2), a key node protein of the osteogenic differentiation regulatory network. The results showed that the red fluorescence intensity of the OSSH-30 and OSSH-50 groups was higher than that of the Ti control, OSSH-100, and Titanium oxide groups, and the surface fluorescence intensity OSSH-30 group was the highest (Fig. 2a). The above results indicate that OSSHs can regulate osteogenic differentiation, and its promotion is closely related to the interval of functional units. At the same time, the quantitative reverse transcription PCR (qPCR) results were consistent with the Runx2 protein expression results. With the decrease of the Schottky functional unit interval, the gene expression level of Runx2 gradually rose. In addition, the expression of Runx2 further promoted the expression levels of other osteogenic related genes (BMP-2, Col-I, Ocn), among which the expression levels of BMP-2, Col-I, and Ocn in the OSSH-30 group were 28.3, 7.4 and 6.9 times of the Ti control group, respectively (Fig. 2c-e). The above experimental results indicate Schottky

heterojunction functional unit has good biocompatibility, can improve the adhesion ability of BMSCs, and enhance the osteogenic differentiation ability of BMSCs at the gene and protein levels.

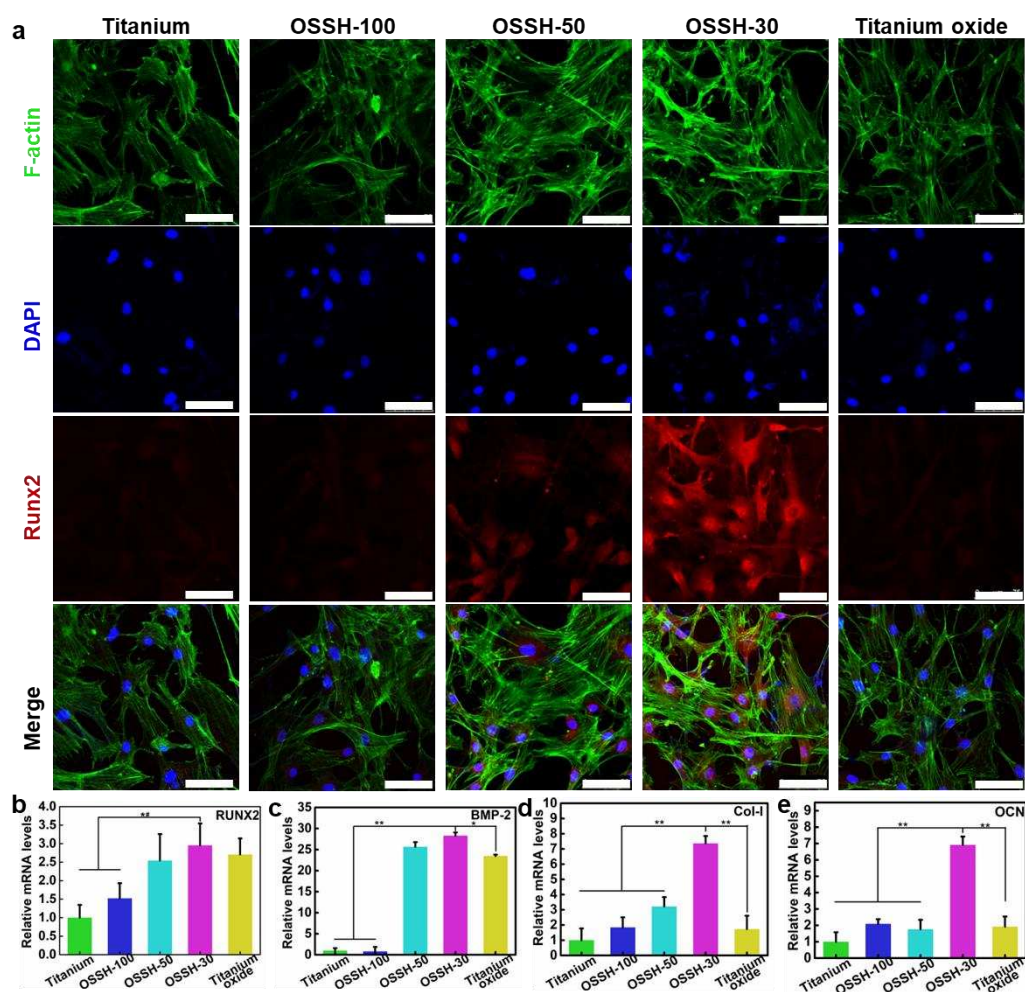


Fig. 2. Osteogenic evolution of BMSCs cultured on OSSHs. (a) Immunofluorescence images of the osteogenic protein Runx2 (red color), actin (green color), nucleus (blue color) and merged channel of BMSCs cultured on different surfaces for 3 days. Scale bar: 75 μ m. (b)-(e) The Osteogenesis-related gene (Runx2, BMP-2, Col-I, OCN) expression results of BMSCs cultured on the surface of different samples. (* $P < 0.05$, ** $P < 0.01$)

Ca^{2+} is a secondary messenger involved in multiple signal transduction pathways. Studies have shown that one of the direct responses of cells to electrical stimulation is the change in intracellular Ca^{2+} concentration[15, 16]. Ca^{2+} mediated signal transduction regulates many different cellular processes

and affects nearly every aspect of cellular life[17, 18]. The external electrical stimulation has been demonstrated to directly regulate the intracellular Ca^{2+} concentration and related cell activities[19, 20]. In order to reveal the potential mechanism of Schottky heterojunction functional unit implant materials in regulating the osteogenic differentiation of BMSCs, we analyzed the intracellular Ca^{2+} concentration and the activation of related downstream signaling pathways. After seeding BMSCs on the surface of OSSHs for 1 day, the observed intracellular Ca^{2+} staining is shown in Fig. 3a. Semi-quantitative fluorescence intensity analysis showed that the Ti control group had the lowest fluorescence intensity (Fig. S4). The fluorescence intensity of OSSH-30 group was the highest, which was 2.22 times that of the Ti group. These results demonstrate that the electrical signals produced by the Schottky heterojunction can directly regulate intracellular calcium and thus regulate cell behavior.

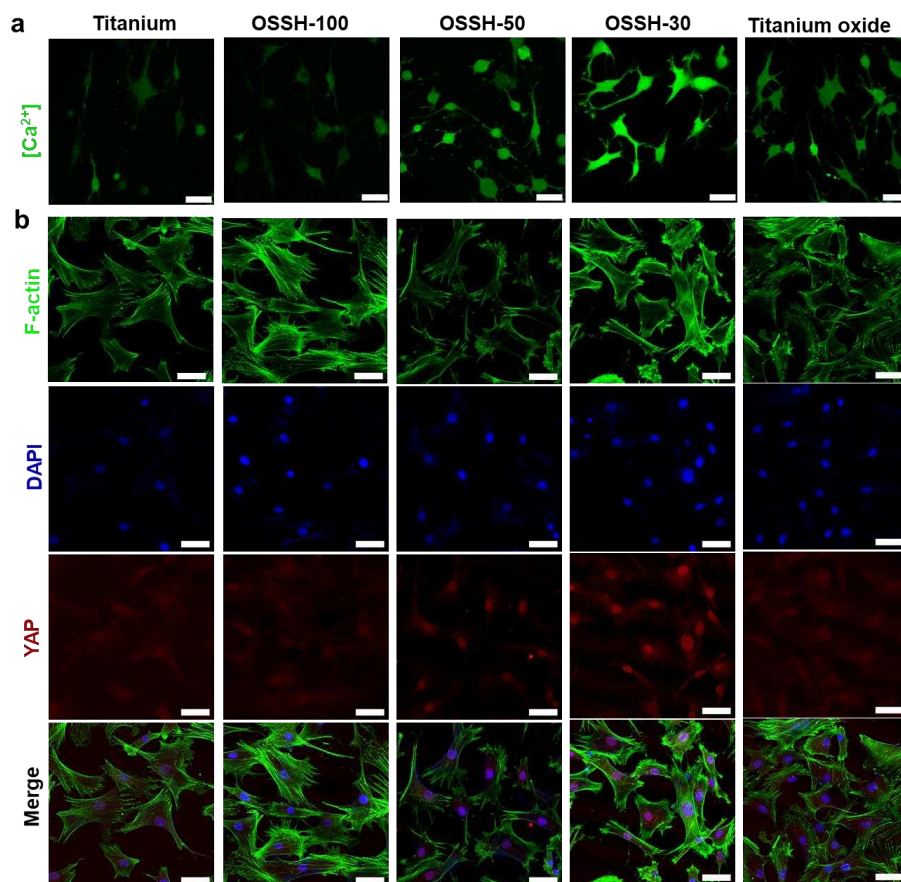


Fig. 3. Fluorescent image of intracellular Ca^{2+} and YAP. (a) The intracellular Ca^{2+} ($[\text{Ca}^{2+}]$) fluorescence

images of BMSCs on different sample surfaces. Scale bar: 25 μm . (b) Immunofluorescence images of YAP nucleus translocation of BMSCs on the surface of different samples. Scale bar: 50 μm .

As the Schottky heterojunction microdomain interval decreases, the electrical signals of the microdomain promotes the increase of intracellular calcium, thereby regulating the activation of downstream signaling pathways. Yes-associated protein (YAP) transcriptional regulator nuclear localization is closely related to mechanotransduction of stem cell[21]. The fluorescence intensity of YAP in the nucleus of the OSSH-30 group was the highest, and the expression of the YAP gene was significantly increased in OSSH-30 group compared to the Ti group (Fig. 3b, Fig. S5). The above results suggest that the Schottky heterojunction of functional units can promote the osteogenic differentiation of stem cells by regulating intracellular calcium ions messenger and mechanobiological pathways.

3.3 OSSH regulates macrophage polarization

When an implant enters the human body, it first interacts with immune cells in the blood to generate an immune response that provides the basic regulatory signals for bone formation process[22]. Among them, macrophages play an important role in the immune regulation of early osteogenesis, and recent studies have shown that macrophage polarization and secretion of biological factors have important regulatory effects on bone regeneration[23]. Depending on different extracellular signals or stimuli, macrophages can polarize to either an M1 or M2 phenotype. M1 type macrophages secrete pro-inflammatory cytokines (such as TNF- α , iNOS, IL-6, etc.), which can promote inflammation and tissue degradation; M2 type macrophages secrete anti-inflammatory cytokines (such as IL-10, TGF- β , etc.), which can enhance angiogenesis and tissue repair[24, 25]. In order to study the immune response of the Schottky heterojunction functional unit implant material, macrophages were seeded on the surface

of OSSHs and cultured for 3 days, and cytoskeleton was stained to observe the cell morphology. As shown in Fig. S6a, the number of macrophages in the Ti group is slightly less than that in the other groups, but the morphology of the macrophages in all the experimental groups and the control group was similar. The results of CCK-8 detection of cell proliferation showed that there was no significant difference in cell proliferation on the surface of each group after 1 day culture. But with the prolongation of culture time, the cell viability generally increased after 4 days of culture. The OSSH-30 group had the highest cell activity, indicating that the introduction of the Schottky heterojunction functional units could promote the proliferation of macrophages.

In order to further study the regulation effect of Schottky heterojunction functional unit implant material on macrophage polarization, flow cytometry was used to detect the expression of markers on the macrophage membrane and determine the phenotype of macrophages. The CCR7 and CD206 are markers on the membrane of M1 and M2 macrophages, respectively. Macrophages cultured on the surface of the Schottky heterojunction functional units were implanted with increased M2 receptor expression (CD206), but decreased M1 receptor (CCR-7) (Fig. S6c,d). Compared with the Ti control group, the sample groups with different electrical functional unit microdomain intervals: OSSH-100, OSSH-50 and OSSH-30 groups down-regulated the proportion of CCR7-positive macrophages and increased the proportion of CD206-positive macrophages, with the OSSH-30 group increased the proportion of CD206-positive macrophages to the highest value of ~ 76.8%. By comparing the ratio of M1/M2 phenotype macrophages on the material surface, it can be concluded that more M1 phenotype macrophages were induced on the surface of the Ti control group, which may cause severe inflammation, while the OSSH-30 surface induces fewer M1 phenotype macrophages, which is more conducive to reducing inflammation, and introduction of more M2 phenotype macrophages has

beneficial effects on the middle and late stages of osseointegration.

Next, pro- and anti-inflammatory proteins secreted by macrophages under different OSSHs was detected via immunofluorescence staining. The results showed that the expression of pro-inflammatory related protein iNOS was higher in Ti control group and OSSH-100 group, while the expression of pro-inflammatory related protein iNOS in OSSH-50 group and OSSH-30 group was lower, and OSSH-30 group showed the least expression (Fig. 4a). Likewise, the immunostaining images of the anti-inflammatory-related protein Arg-1 showed that the expression of the anti-inflammatory related protein Arg-1 was higher in the OSSH-50 group and the OSSH-30 group than in the other groups (Fig. 4b). Among them, the OSSH-30 group expressed the most, which indicates that the OSSH-30 can reduce inflammation and promote tissue repair. The expressions of tumor necrosis factor- α (TNF- α) and Interleukin-10 (IL-10), the typical pro- and anti-inflammatory factors, were also significantly decreased and increased, respectively, in OSSH-30 group (Fig. 4c, d)[16, 26, 27]. Transforming growth factor- β (TGF- β) and Platelet derived growth factor (PDGF), cytokines produced by macrophages to induce osteoblast migration, proliferation or the secretion of bone extracellular matrix early in differentiation, were also increased in OSSH-30 group (Fig. 4e, f)[28, 29]. The expression levels of PDGF and TGF- β were not significantly different in the Ti control, OSSH-100 and Titanium oxide groups, whereas the expression levels were up-regulated in the OSSH-50 and OSSH-30 groups. The expression levels of PDGF in the OSSH-50 and OSSH-30 groups were 2.95 and 6.45 times that of the Ti control group, respectively. The above results confirm that the functional unit structured material can regulate the anti-inflammatory M2 expression of macrophages and create a favorable immune microenvironment for bone regeneration.

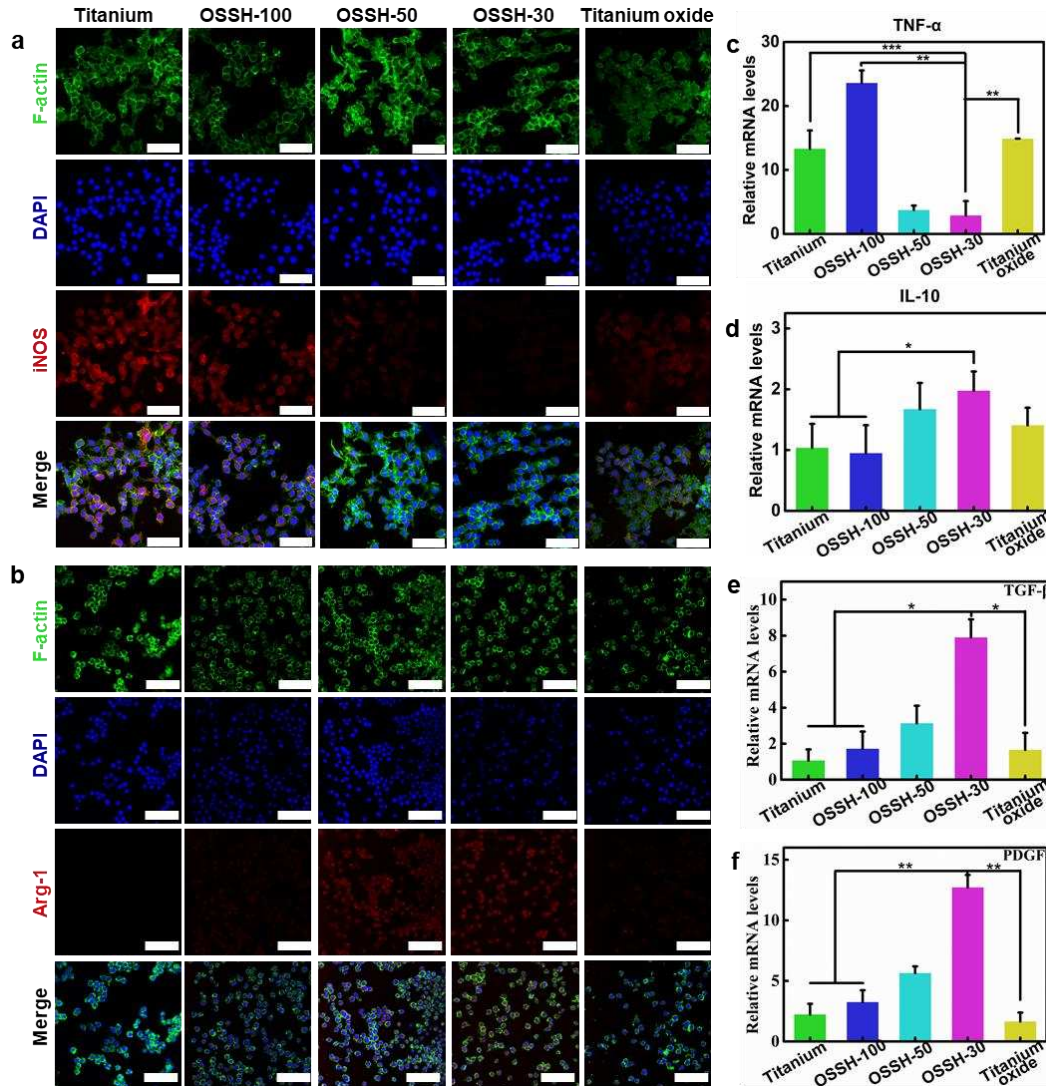


Fig. 4. Macrophage polarization on OSSHs. (a) and (b) Immunofluorescence staining image of macrophages on OSSHs with the pro-inflammatory (M1 type) related protein iNOS and the anti-inflammatory (M2 type) related protein Arg-1. Scale bar: 75 μm. (c)-(e) RT-qPCR detection results of inflammation-related genes (M1: TNF-α. M2: IL-10) of macrophages cultured on the surface of different samples for 3 days. (f) and (h) RT-qPCR detection results of TGF-β and PDGF of macrophages cultured on the surface of different samples for 3 days. (*P<0.05, **P<0.01, ***P<0.001, vs. Ti group).

Science the OSSHs promoted M2 expression and osteogenic growth factors secretion from macrophages, we further cultured BMSCs using macrophage-conditioned medium to detect osteogenic

differentiation (Fig. 5a). Both qualitative ALP staining results and quantitative ALP activity kit examination results showed that OSSH-30 group had the highest ALP expression (Fig. 5b, c). And the results of immunofluorescence staining of osteogenic differentiation-related protein Osteopontin (OPN) showed that the red fluorescence intensity of Ti control, OSSH-100 and TITANIUM OXIDE groups was weak, whereas the OSSH-50 and OSSH-30 groups showed strong red fluorescence, with OSSH-30 showing the highest fluorescence intensity (Fig. 5d). The titanium oxide group shows no Schottky heterojunction functional unit. The macrophage cultured on the laser oxidized group can't transform to the M2 type, and the macrophage mainly secretes inflammatory cytokines, resulting in the poor osteogenic performance of the titanium oxide group. These results of immunofluorescence staining suggested that the macrophages induced by the OSSH-30 group could secrete more cytokines to promote the osteogenic differentiation of BMSCs.

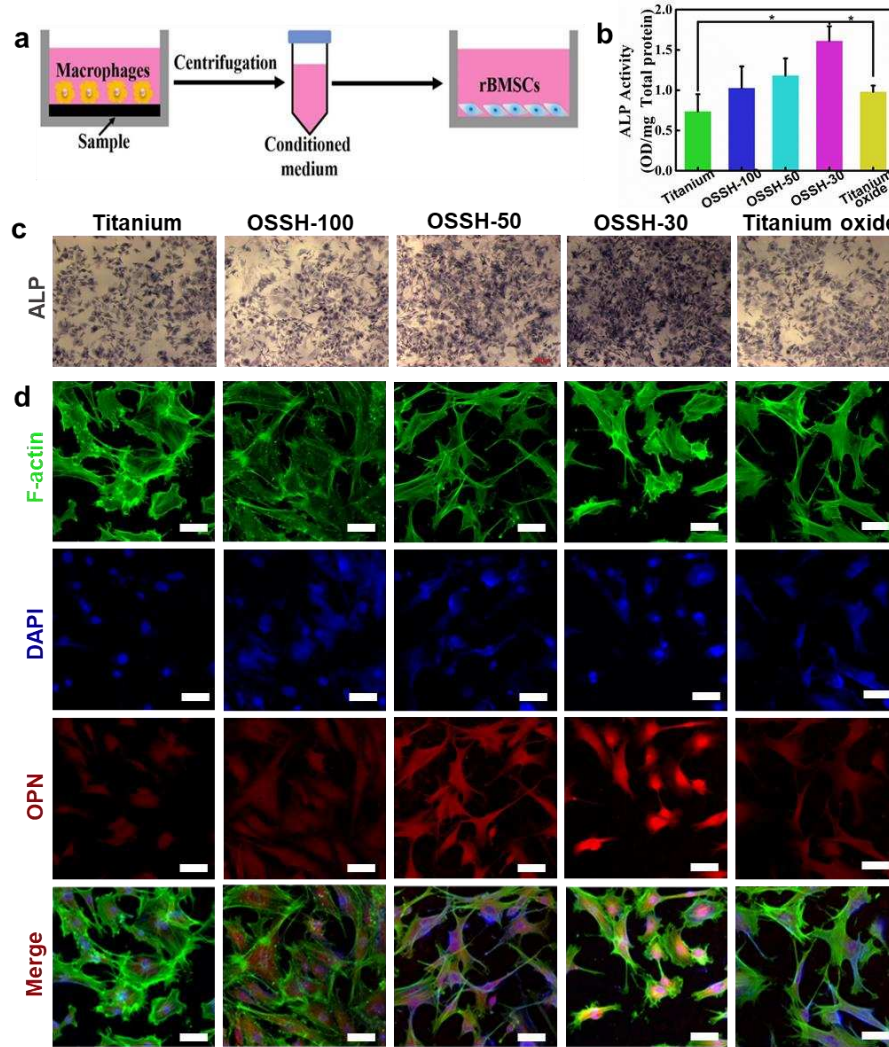


Fig. 5. The differentiation of BMSCs cultured in macrophage-conditioned medium of OSSHs. (a) Schematic illustration of culturing BMSCs using macrophage-conditioned medium. (b) and (c) Quantitative and qualitative detection of ALP after culturing BMSCs in macrophage conditioned medium for 7 days. (* $P < 0.05$) (d) Immunofluorescence image of osteogenic related protein OPN expression after culturing BMSCs in macrophage conditioned medium. Scale bar: 50 μm .

The Schottky heterojunction functional units enable manipulation of the electrical cues on biomaterials to regulate the polarization of macrophages. In order to further explore the potential mechanism by which the electric cues of OSSHs affect the polarization of macrophages, we first detected the intracellular Ca^{2+} concentration of macrophages by Ca^{2+} staining. Only a few cells in the Ti control

group and Titanium oxide group showed weak green fluorescence, while the green fluorescence intensity of the OSSH-100, OSSH-50, and OSSH-30 groups increased compared to Ti control, and OSSH-30 group showed the highest fluorescence intensity, indicating the highest intracellular Ca^{2+} concentration (Fig. 6a). To explore the effect of increased intracellular Ca^{2+} concentration of macrophages on downstream signaling pathways, we used RT-qPCR to detect the expression levels of genes related to the PI3K/AKT/mTOR signaling pathway which has been demonstrated to be activated under electric stimulation from external electric facility[8, 30]. The results showed that PI3K and mTOR were most expressed in the OSSH-30 group (Fig. 6b, c). The expression levels of AKT in the OSSHs groups were significantly up-regulated, with OSSH-30 group up-regulated by 2.264 times compared to the Ti control group (Fig. 6d). These results indicate that OSSH activates Ca^{2+} influx, and further enhances the PI3K/AKT/mTOR signaling pathway to polarize macrophages to M2 type, secretes more cytokines that promote tissue repair, and then form an immune microenvironment conducive to the differentiation of stem cells.

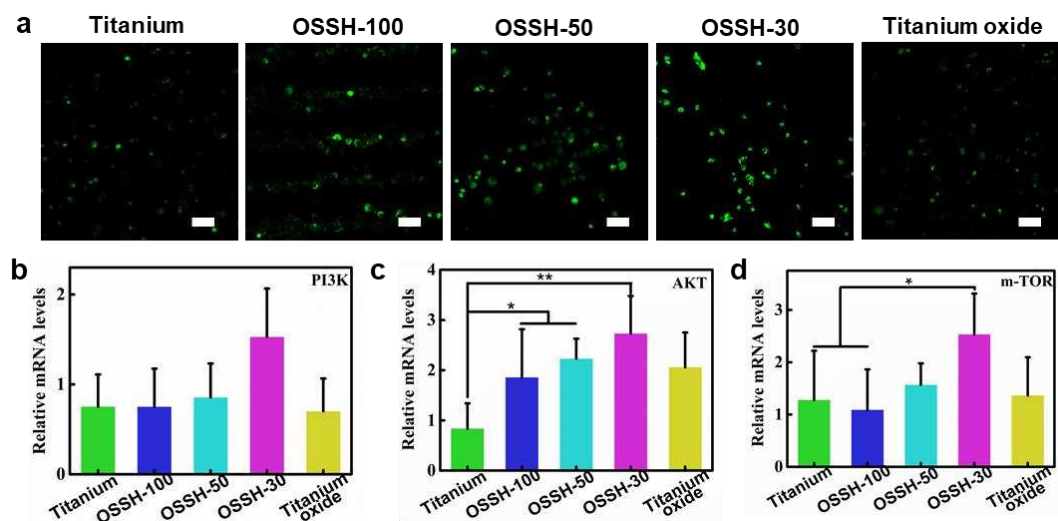


Fig. 6. Exploration of intracellular signals of OSSH groups. (a) and (b) Fluorescence images and semi-quantitative statistics of macrophages stained for detection of intracellular Ca^{2+} concentration on the surface of different samples. Scale bar: 50 μm . (c) RT-qPCR expression results of PI3K/AKT/mTOR

signaling pathways of macrophages on the surface of different samples (*P<0.05, **P<0.01)

3.4 OSSH regulates bone regeneration *in vivo*

Finally, the osteogenic performance of OSSH material was verified by *in vivo* rat femur defect implant experiments. A cylindrical OSSH titanium implant material with a diameter of 2 mm was implanted into the corresponding femoral defect site. One month after implantation, micro-CT three-dimensional reconstruction analysis was performed. The results showed that a larger amount of new bone was formed on the surface of the OSSH-30 group compared to control groups (Fig. 7). Further quantitative analysis of BV/TV, Tb.N, and Tb.Th of new bone formation confirmed that OSSH-30 group possess the quality of surrounding bone formation (Fig. S7). The growth of peri-implant tissue was further analyzed by hematoxylin-eosin (HE) staining and Masson trichrome staining, which shows that the OSSH surface was covered by newly formed bone tissues (red). In contrast, hardly any bone tissue can be observed to be in-contact with implant. It can be seen from the bone defect healing process that the immune microenvironment regulated of immune cells is very important to the bone defect healing process.

A poor immune response can lead to chronic inflammation at the implant site will result, which can cause fiber to wrap around the implant, making it difficult for the implant to form osteointegration with the bone tissue. The enlarged image of HE staining shows that there is serious fiber envelopment between pure titanium and bone tissue (Fig. 7). However, the OSSH group did not form obvious fiber wrap around, but formed a good interface with bone tissue. There are still fiber wraps around the Titanium oxide group, and the amount of bone formation at the interface is low. The above results are consistent with the response results of immune cells and bone marrow mesenchymal stem cells *in vitro*. It is proved that the Schottky functional unit structure has the function of regulating immunity and promoting bone formation.

In this study, an implant design concept of order structure with functional units was proposed. This innovative concept will inspire future development of micro- and nanoscale semiconductive ordered structures with functional units, with the aid of advanced material synthesis and preparation technologies. Furthermore, the bone implant with ordered structure with functional units will be promoted toward precision and controllability.

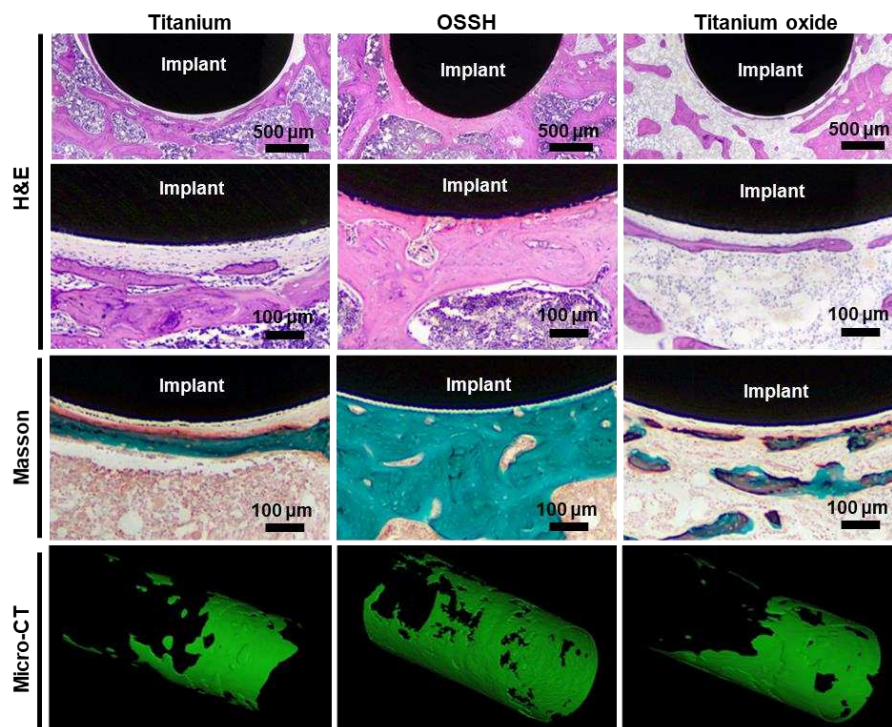


Fig. 7. *In vivo* OSSH implant in the femoral defect and its osteogenic performance. Hematoxylin-eosin staining of tissue sections at 6 weeks after implantation. Masson's trichrome staining of histological sections at 6 weeks after implantation. Representative 3D Micro-CT reconstruction of the newly formed bone around the OSSH and control implant 6 weeks post-implantation.

4. Conclusion

In this research, ordered structures with Schottky heterojunction functional unit were developed on titanium implants via selective microdomain oxidation to modulate bone regeneration. The Schottky heterojunction functional unit possess a surface potential difference of ~ 50 mV between the oxidized

microdomain and original titanium microdomain, and the oxidized microdomain were demonstrated to be n-type semiconductors with a higher charged carrier density, which provided a unique electric microenvironment to regulate bone regeneration. *In vitro* cell culture and examination experiment indicated that the OSSH-30 had good biocompatibility, can improve the adhesion ability of BMSCs, and enhance the osteogenic differentiation ability of BMSCs at the gene and protein level via mechanotransduction signal pathways. Moreover, the OSSH-30 is demonstrated to reduce inflammation around titanium implant via inducing more M2 phenotype macrophages and less M1 phenotype macrophages via promoting Ca^{2+} influx, and further activating the PI3K/AKT/mTOR signaling pathway, which further benefits osseointegration. *In vivo* bone defect implant experiment also demonstrated that the OSSH-30 can promote bone regeneration. Our research provides a new strategy via developing ordered structures with electric functional units to regulate tissue regeneration.

Acknowledgements

This work is financially supported by the National Natural Science Foundation of China (Nos. 52072127, 52201297, U21A2055 and U22A20160), the China Postdoctoral Science Foundation (No. 2022M711200), the Royal Society (IEC/NSFC/191344) (UK).

Conflict of Interest

The authors declare no conflict of interest.

Data availability

The raw data required to reproduce these findings cannot be shared at this time due to technical or time limitations

References

- [1] H. Fukui, R.W.Y. Chow, J. Xie, Y.Y. Foo, C.H. Yap, N. Minc, N. Mochizuki, J. Vermot, *Science* 374 (6565) (2021) 351-354.
- [2] M. Levin, *Cell* 184 (8) (2021) 1971-1989.
- [3] Y. Zhao, Y. Liang, S. Ding, K. Zhang, H. Mao, Y. Yang, *Biomaterials* 255 (2020) 120164.
- [4] B. Ferrigno, R. Bordett, N. Duraisamy, J. Moskow, M.R. Arul, S. Rudraiah, S.P. Nukavarapu, A.T. Vella, *Bioact. Mater.* 5 (3) (2020) 468-485.
- [5] Z. Li, G. Li, X. Wang, Z. Zhao, *J. Mater. Sci. Technol.* 172 (2024) 228-239.
- [6] X. Zhang, T. Wang, Z. Zhang, H. Liu, L. Li, A. Wang, J. Ouyang, T. Xie, L. Zhang, J. Xue, W. Tao, *Mater. Today.* 68 (2023) 177-203.
- [7] J. Zheng, J. Zuo, C. Xiao, Q. Guo, X. Fu, C. Ning, P. Yu, *J. Mater. Sci. Technol.* 168 (2024) 24-34.
- [8] Y. Liu, X. Zhang, C. Cao, Y. Zhang, J. Wei, Y. Li, W. Liang, Z. Hu, J. Zhang, Y. Wei, X. Deng, *Adv. Funct. Mater.* 27 (47) (2017).
- [9] C.P. Brown, J.L. Boyd, A.J. Palmer, M. Phillips, C.A. Couture, M. Rivard, P.A. Hulley, A.J. Price, A. Ruediger, F. Légaré, A.J. Carr, *Adv. Funct. Mater.* 26 (42) (2016) 7662-7667.
- [10] N. Reznikov, M. Bilton, L. Lari, M.M. Stevens, R. Kroger, *Science* 360 (6388) (2018) eaao2189.
- [11] E. Gachon, P. Mesquida, *Acs. Nano.* 15 (6) (2021) 9820-9826.
- [12] C. Halperin, S. Mutchnik, A. Agronin, M. Molotskii, P. Urenski, M. Salai, G. Rosenman, *Nano. Lett.* 4 (7) (2004) 1253-1256.
- [13] K. Chen, L. Li, *Adv. Mater.* 31 (32) (2019) 1901115..
- [14] E.G. Long, M. Buluk, M.B. Gallagher, J.M. Schneider, J.L. Brown, *Bioact. Mater.* 4 (2019) 249-255.
- [15] S.J.Han, M. Noh, J.H. Jang, J.B. Lee, K.S. Kim, *J. Cell. Physiol.* 236 (11) (2021) 7450-7463.
- [16] Q. Yang, S. Kajimoto, Y. Kobayashi, H. Hiramatsu, T. Nakabayashi, *J. Phys. Chem. B.* 125 (38) (2021) 10692-10700.
- [17] C. Galli, G. Pedrazzi, S. Guizzardi, *Bioelectromagnetics* 40 (4) (2019) 211-233.
- [18] H. Lee, K.M. Cho, M.K. Kim, M. Lee, H. Kim, C.Y. Choi, K.K. Kim, J.S. Park, H.H. Kim, Y.S. Bae, *J. Cell. Mol. Med.* 25 (1) (2021) 473-483.
- [19] X. Huang, J. Xing, Z. Wang, J. Han, R. Wang, C. Li, C. Xiao, F. Lu, J. Zhai, Z. Zhou, Y. Li, L. Zhou, Z. Song, D. Chen, P. Yu, C. Ning, X. Jiang, *Adv. Funct. Mater.* 31 (50) (2021) 2106249.
- [20] G. Thirvikraman, S.K. Boda, B. Basu, *Biomaterials* 150 (2018) 60-86.
- [21] Y. Zhao, Q. Sun, B. Huo, *Biomater. Transl.* 2 (4) (2021) 312.
- [22] Z.T. Chen, T. Klein, R.Z. Murray, R. Crawford, J. Chang, C.T. Wu, Y. Xiao, *Mater. Today.* 19 (6) (2016) 304-321.
- [23] W. Qiao, H. Xie, J. Fang, J. Shen, W. Li, D. Shen, J. Wu, S. Wu, X. Liu, Y. Zheng, K.M.C. Cheung, K.W.K. Yeung, *Biomaterials* 276 (2021) 121038.
- [24] X. Dai, B. Heng, Y. Bai, F. You, X. Sun, Y. Li, Z. Tang, M. Xu, X. Zhang, X. Deng, *Bioact. Mater.* 6 (7) (2021) 2029-2038.
- [25] R. Liu, S. Chen, P. Huang, G. Liu, P. Luo, Z. Li, Y. Xiao, Z. Chen, Z. Chen, *Adv. Funct. Mater.* 30 (21) (2020) 1910672.
- [26] Z. Zheng, Y. Chen, D. Wu, J. Wang, M. Lv, X. Wang, J. Sun, Z. Zhang, *Theranostics* 8 (19) (2018) 5482-5500.
- [27] P. Zhou, D. Xia, Z. Ni, T. Ou, Y. Wang, H. Zhang, L. Mao, K. Lin, S. Xu, J. Liu, *Bioact. Mater.* 6 (3) (2021) 810-822.
- [28] A.N. Rindone, B. Kachniarz, C.C. Achebe, R.C. Riddle, A.N. O'Sullivan, A.H. Dorafshar, W.L.

Grayson, *Adv. Healthc. Mater.* 8 (10) (2019) 1801565.

[29] X. Wen, K. Xi, Y. Tang, J. Bian, Y. Qin, W. Xiao, T. Pan, X. Cheng, Z. Ge, W. Cui, *Small* 19 (15) (2023) 2207030.

[30] L. Fan, C. Xiao, P. Guan, Y. Zou, H. Wen, C. Liu, Y. Luo, G. Tan, Q. Wang, Y. Li, P. Yu, L. Zhou, C. Ning, *Adv. Healthc. Mater.* 11 (1) (2022) 2101556.